



**University of Dundee**

**Experimental and numerical investigations on buckling behaviour of stiffened panel during creep age forming**

Zhou, Wenbin; Shi, Zhusheng; Rong, Qi; Bai, Xuepiao; Zeng, Yuansong; Lin, Jianguo

*DOI:*

[10.1016/j.tws.2022.108940](https://doi.org/10.1016/j.tws.2022.108940)

*Publication date:*

2022

*Licence:*

CC BY

*Document Version*

Publisher's PDF, also known as Version of record

[Link to publication in Discovery Research Portal](#)

*Citation for published version (APA):*

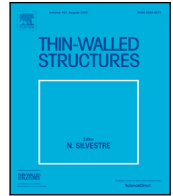
Zhou, W., Shi, Z., Rong, Q., Bai, X., Zeng, Y., & Lin, J. (2022). Experimental and numerical investigations on buckling behaviour of stiffened panel during creep age forming. *Thin-Walled Structures*, 172, Article 108940. <https://doi.org/10.1016/j.tws.2022.108940>

**General rights**

Copyright and moral rights for the publications made accessible in Discovery Research Portal are retained by the authors and/or other copyright owners and it is a condition of accessing publications that users recognise and abide by the legal requirements associated with these rights.

**Take down policy**

If you believe that this document breaches copyright please contact us providing details, and we will remove access to the work immediately and investigate your claim.



Full length article

## Experimental and numerical investigations on buckling behaviour of stiffened panel during creep age forming

Wenbin Zhou<sup>a</sup>, Zhusheng Shi<sup>a,\*</sup>, Qi Rong<sup>a</sup>, Xuepiao Bai<sup>b</sup>, Yuansong Zeng<sup>b</sup>, Jianguo Lin<sup>a</sup>

<sup>a</sup> Department of Mechanical Engineering, Imperial College London, London SW7 2AZ, UK

<sup>b</sup> AVIC Manufacturing Technology Institute, Beijing 100024, China

### ARTICLE INFO

#### Keywords:

Buckling  
Stiffened panel  
Four point bending  
Creep age forming  
Finite element modelling

### ABSTRACT

Experimental and numerical studies on the buckling behaviour of stiffened panels under four point bending during creep age forming (CAF) have been carried out in this study for the first time. The experimental programme comprised buckling tests of five different sizes of stiffened panels of aluminium alloy 7050 at room temperature and buckling tests with different loading degrees in CAF including the loading, heating and creep-ageing stages. The buckling mode, the strain distribution and the strain evolution of the stiffened panel were obtained from the experiments, using digital image correlation (DIC) for the room temperature tests and strain gauges for the CAF tests. The effect of stiffener height and stiffener thickness and the effect of the heating and creep-ageing stages in CAF on the buckling behaviour have been investigated and discussed. It was found that buckling mode varied from one half-wave cosine mode in the elastic loading to three half-wave cosine mode with the increase of buckling stress from elastic to plastic region, and during CAF buckling mainly occurred and grew in the heating process. The corresponding non-linear finite element (FE) simulations of stiffened panels at room temperature and ageing temperature (160 °C) have also been carried out, and the FE results of buckling strain and buckling mode shape show a good agreement with experimental results. The non-linear FE method can provide accurate results of buckling strain and formability limits for cold forming and CAF processes, which can be used to guide the structural design of stiffened panels.

### 1. Introduction

Lightweight is of great importance in many industries, especially for transportation vehicles. Integrally stiffened panels, one of lightweight structures, are widely applied in aerospace and marine applications due to their advantages of high bending stiffness and high resistance to crack growth [1,2]. Creep age forming (CAF), which combines the forming operation and heat-treatment, has been reported to be an appropriate method for forming the flat stiffened aluminium panels into desired shapes with certain curvature [3,4]. CAF can concurrently shape and strengthen workpieces at an ageing temperature through creep deformation and artificial ageing. Compared with the conventional forming methods such as roll forming and shot peen forming, the CAFed panels have low residual stress and high strength [5,6]. The procedures of CAF process can generally be divided into three stages: loading, creep-ageing (including heating) and unloading, as shown in Fig. 1. In CAF process, the workpiece can be loaded with tools at room temperature and then the workpiece with tools is placed in the furnace to heating to ageing temperature and held at the constant temperature for a period of time before unloading. Since CAF are widely applied in the manufacture of large panel components with

small curvature, elastic bending is generally applied in the loading stage of CAF process [5]. However, for CAF of stiffened panel, the loading on stiffener may enter the plastic region.

During the CAF process, global bending is the general applied loading condition for stiffened panels. Buckling may occur on the stiffener of the stiffened panel in the loading or creep-ageing stages due to the high concentrated compressive stress at the top of the stiffener from the global bending and the material property changing with temperature and time, which will cause dimensional deviation and reduce the strength of the stiffened panel [5,8]. Buckling is one of the challenges in CAF of stiffened panels and it is significant to experimentally investigate the buckling behaviour of stiffened panels subjected to bending in the loading stage and heating and creep-ageing stages of CAF and built finite element (FE) model to predict the behaviour, in order to guide the design of stiffened panels and avoid possible buckling in the forming process.

Finite element (FE) method has been used to obtain buckling behaviour of stiffened panels under uniform compression and bending [9, 10]. Eigenvalue FE buckling analysis and non-linear FE buckling analysis are two main FE methods to predict the buckling characteristics.

\* Corresponding author.

E-mail address: [zhusheng.shi@imperial.ac.uk](mailto:zhusheng.shi@imperial.ac.uk) (Z. Shi).

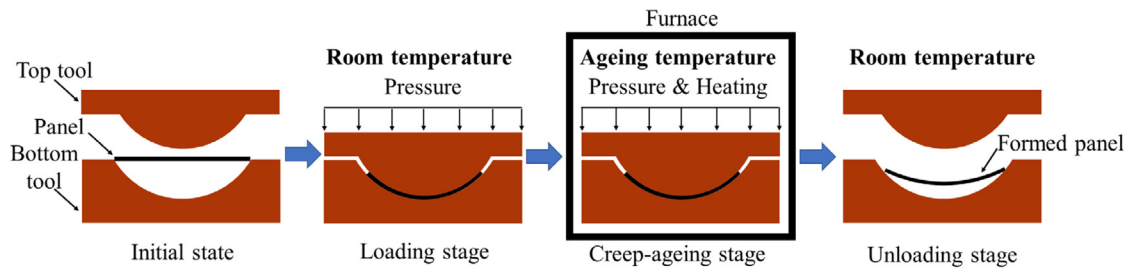


Fig. 1. Schematic showing procedure of CAF process.  
Source: (modified from [7]).

The eigenvalue buckling method can simulate the buckling mode and predict the buckling stress of the workpiece by solving an equilibrium equation [11]. The eigenvalue buckling method has been applied in studies on the prediction of buckling strength of stiffened panels, such as the elastic local buckling strength of T-stiffened panels with a wide range of typical panel geometries subjected to uniaxial compression [12] or biaxial thrust [13]. However, it cannot be used in applications with any plastic strain since the stiffness matrices used in the equilibrium equation is linear elastic and non-linear material properties (plasticity) are ignored in the method [14].

Non-linear buckling method can provide the buckling and post-buckling behaviour in both elastic and plastic regions, in which the plasticity of the material can be considered. However, the time consumption in the non-linear buckling method is much longer than that in the eigenvalue buckling method. An initial geometric imperfection is necessary to be introduced in the non-linear buckling method to drive the beginning of buckling. The initial imperfections have several different methods to consider in the non-linear buckling method, such as: the deflection from the elastic buckling modes [9,15], the superposition of the Fourier components [16], the deformation of the structure subjected to uniform lateral pressure [17] and measured imperfection of the experimental workpiece [18]. The non-linear buckling analysis has been applied to investigate the buckling strength of stiffened panels subjected to different loading conditions in many published works. The effect of the geometries and boundary conditions of the stiffened panels [19,20] and the effect of friction stir weld [21] on the buckling and post-buckling behaviour of stiffened panels under uniform compression has been investigated, in which the welding heat-affected zone (HAZ) and welding residual stresses were considered in the FE model. Parametric studies on the buckling response of stiffened panels with T-shape stiffener [22] and blade stiffener [23] loaded with bending moments have been investigated, in which the stiffener height and thickness have been found to be the most influential parameter affecting the buckling stress of stiffened panel. However, the buckling behaviour of orthogrid stiffened panels under bending, which is important for the design and manufacture of panels in the transportation industry, is rarely studied in literature.

Experimental investigation for buckling and post-buckling behaviour of flat integrally stiffened panel with different shapes of stiffeners under axial compression has been reported in many literature works, such as T-stiffener [24], I-stiffener [25], blade stiffener [26], L-shape and hat-shape stiffeners [27], in which several buckling modes have been found including the regular buckling of the entire panel, skin buckling and stiffener tripping. The increase of the equivalent compression stiffness of stiffener enhances the buckling load but has little influence on the failure load. In these experiments, the difference of the strain of the structure is captured using strain gauges [28] or a digital image correlation (DIC) system to study the buckling behaviour. Compared with strain gauges which can only obtain the average strain of the strain gauge attached area, DIC system can measure the whole strain field for the measured area. Other methods to obtain buckling behaviour are to measure the out-of-plane deflection using Moire screen [29], linear voltage differential transducer (LVDT) [30] and 3D-DIC [31].

Table 1

Main chemical compositions of AA7050 (wt.%).

Zn	Cu	Mg	Zr	Fe	Si	Ti	Mn	Cr	Al
6.2	2.3	2.3	0.13	0.03	0.02	0.02	0.004	0.001	Bal.

Up to now, however, no report has been found for the experimental investigation of buckling behaviour for integrally stiffened panels under out-plane bending or non-uniform stress.

Therefore, in this study, the buckling behaviour of aluminium alloy stiffened panels subjected to four point bending in the loading stage and the whole process of CAF was experimentally investigated for the first time to study the formability limits due to buckling for cold forming process and CAF. DIC system and strain gauge were used to capture the buckling mode, buckling strain and buckling stress of stiffened panel under bending. Non-linear FE simulations have been conducted and the results are compared with the corresponding experimental results. Finally, the effects of the stiffener height and stiffener thickness of stiffened panels and the effects of the heating and creep-ageing stages in CAF on the buckling mode and buckling strain have been investigated based on the experimental and numerical results.

## 2. Experimental procedure

### 2.1. Material and properties

The material used for the stiffened panels in this study was aluminium alloy 7050 (AA7050), which is a high strength aluminium alloy typically used in the fuselage frames and wing skins for aircraft. The chemical composition of the material is listed in Table 1. The as-received AA7050 was in T7451 temper condition, which was achieved by solution heat-treatment at 475 °C for 1 h, water-quenching, pre-stretching, and artificial ageing at 115 °C for 8 h followed by artificial ageing at 165 °C for 16 h [32].

Uniaxial tensile tests at room temperature and the ageing temperature of 160 °C were conducted with a loading strain rate of  $2.5 \times 10^{-4} \text{ s}^{-1}$  to obtain the basic tensile properties of AA7050-T7451, following the ASTM standards E8/E8M-21 and E21-17 [33,34]. Cylindrical specimens were used with a diameter of 8 mm and a length of 51 mm in the gauge length area. Three tests were repeated for each temperature. The engineering stress-strain curves of the as-received material are shown in Fig. 2, which demonstrates decreased strength at the ageing temperature. The 0.2% offset yield strength of the material was 489 MPa at room temperature and 386 MPa at 160 °C, with a standard deviation of 2.4 and 3.2 MPa, respectively. The Young's modulus of the material at room temperature and ageing temperature was 68 GPa [35].

### 2.2. Stiffened panel specimens

The buckling behaviour of stiffened panels under four point bending in creep age forming is investigated in this paper. The stiffened panel

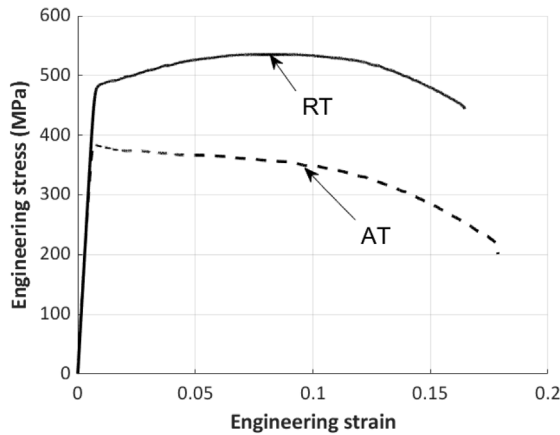


Fig. 2. Engineering stress–strain curves of AA7050-T7451 material at room temperature (RT, solid line) and ageing temperature of 160 °C (AT, dashed line).

specimens used in the present study are the orthogrid stiffened panel with one longitudinal blade stiffener and two transverse blade stiffeners. The schematic diagram of the stiffened panel specimen is shown in Fig. 3. Five groups of stiffened panel specimens with different stiffener height  $h$  and the stiffener thickness  $t_{st}$  were designed for this study, P1–P5, since the plastic buckling of the stiffened panel was mainly sensitive to the stiffener height  $h$  and the stiffener thickness  $t_{st}$  [36,37]. The geometric parameters for the five groups of specimens are also listed in Fig. 3, which were designed to cover both elastic buckling and plastic buckling in the tests. The stiffened panel specimens have a total length  $3a$  of 300 mm, width  $b$  of 65 mm, and the same skin thickness  $t_{sk}$  and stiffener thickness  $t_{st}$ . The specimens P1, P2 and P3 had a same stiffener thickness of 3 mm and different stiffener heights as 30, 35 and 40 mm, respectively, while the specimens P2, P4 and P5 had a same stiffener height of 35 mm and different stiffener thickness as 3, 2.5 and 3.5 mm, respectively. The specimens were machined from the as-received 45 mm thickness AA7050-T7451 plates, with the longitudinal direction of the specimens parallel to the rolling direction of the as-received material.

## 2.3. Experimental setup and test procedure

### 2.3.1. Buckling tests at room temperature

Buckling tests at room temperature were carried out to study the buckling behaviour of the stiffened panel, including buckling mode and buckling stress under bending in both elastic and plastic regions, to study the formability of stiffened panels due to buckling. The data can also be used to evaluate the effectiveness of the finite element model. In the tests, the stiffened panels were loaded until buckling occurs under four point bending, similar to the loading process of CAF.

The buckling tests were conducted on a 250-tonne hydraulic press. A four point bending test rig was used in the buckling tests, and its design is shown in Fig. 4(a). The upper integral rollers with a gap of 6 mm in the middle, as shown in Fig. 4(b), were specifically designed to avoid touching the stiffener during the loading process. The distance between the upper rollers is 60 mm and that for the bottom rollers is 260 mm. Fig. 5 shows the experiment setup of the buckling tests involving stiffened panel specimen, test rig, loading machine and 2D-digital image correlation (2D-DIC) system.

To monitor the buckling behaviour of the stiffened panel specimen during the loading stage, a 2D-DIC technique was used in the room temperature tests to capture the displacement and strain field on the two sides of the longitudinal stiffener of the specimen during the loading process. Random speckle patterns were painted on the measured surfaces of the stiffened panel specimens. The DIC system comprises of two cameras (Canon EOS 80D) with a spatial resolution

of  $1920 \times 1080$  pixels. Two cameras were placed on the two sides of the stiffened panel specimen, as shown in Fig. 5. Videos with 24 frames per second were taken by the two cameras during the loading stage to acquire the deformation and buckling response of the specimens. Two light sources were placed behind the corresponding camera and used to ensure the brightness of the measured surface and reduce image noise. In addition, a continuous video along the longitudinal stiffener direction was recorded using another camera for capturing the buckling behaviour of the stiffened panel specimen. The data from the DIC system was processed for strain evolution using GOM software Correlate 2018, in which the facet size and point distance were set to be  $32 \times 32$  pixels and 27 pixels with 15.6% overlapping.

In the tests, four point bend load was applied on the specimen by the loading machine pressing down the top frames of the test rig through a load transmission cylinder. The loading with displacement control mode was applied with a crosshead speed of 1 mm/min until an observable buckling occurs on the longitudinal stiffener of the specimen.

### 2.3.2. Buckling tests in creep age forming progress

Buckling tests in creep age forming process were conducted to study the buckling behaviour of stiffened panels during CAF and investigate the effect of heating and creep-ageing on the buckling behaviour. The stiffened panels were loaded to a certain displacement before buckling occurs, and the buckling response of stiffener surfaces of the stiffened panel specimens was monitored during the loading, heating and creep-ageing stages of the CAF process.

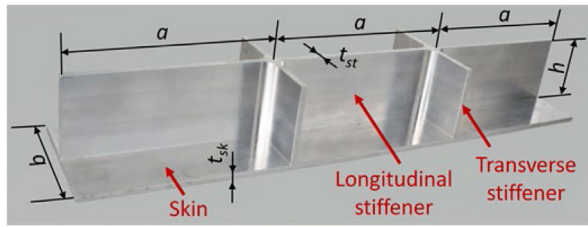
The P2 specimens ( $h = 35.0$  mm,  $t_{st} = t_{sk} = 3.00$  mm) were used in the buckling tests in CAF process. The stiffened panel specimens were loaded to 90% and 100% of the critical buckling strain which was obtained from the buckling tests at the room temperature, and then heated to 160 °C and creep-aged under the constant strain for 16 h with the compression strain at the top of the longitudinal stiffener being monitored using strain gauges.

The loading stage process was the same as that in the room temperature tests. In the heating and creep-ageing stages, a thermocouple was attached on the stiffened panel specimen to monitor the temperature, and the temperature data was recorded via a data logger.

Since the stiffened panel specimen is in the box furnace for creep-ageing and the DIC system cannot be used to monitor the buckling response of the specimen, strain gauges were used to measure the strain. For this, buckling tests at room temperature with strain gauge measurement were conducted to compare the strain measurement performance of the DIC system and strain gauge. The setup of the strain gauge measurement is shown in Fig. 6. High temperature strain gauges having 30 mm integral lead and a temperature range from  $-30$  to  $180$  °C with a gauge resistance of  $120 \Omega$  were used. The strain gauges were bonded on the stiffened panel specimen with M-Bond AE-10 adhesive, which has an upper temperature limit of 204 °C and can cure at room temperature. The location of the strain gauge is presented in Fig. 6 and the distance between the middle line of the strain gauge and the top edge of the stiffener was 5 mm. A P3 strain indicator and recorder supplied by Micro-Measurements was used to record the strain data from the strain gauge in real time. The three-wire quarter-bridge circuit was set up for the strain gauge measurement in the tests, in which the bridge was resistively symmetrical and the temperature change for the wires would not affect the strain data. The bridge was balanced before the buckling tests.

In the tests, the specimen was loaded by four point bending by the loading machine with a constant speed of  $1 \text{ mm} \cdot \text{min}^{-1}$  until the desired displacement was achieved. After loading, the position of top frame of the test rig was locked by bolts and nuts. The whole test rig setup was moved into a box oven to heat up to 160 °C, then creep-aged with constant temperature for 16 h. Finally, the test rig was cooled down to the room temperature and the specimen was then unloaded. The strain of the top stiffener was recorded by the strain indicator and recorder during the loading, heating and creep-ageing stages.

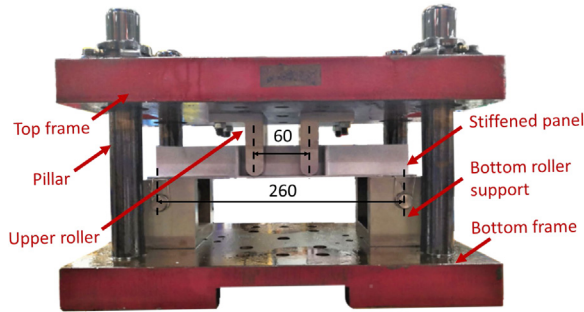




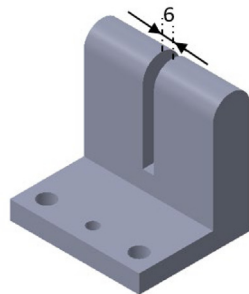
**Geometric parameters of the orthogrid stiffened panels**

Specimen	Geometric parameters (unit: mm)		
	$h$	$t_{sk}$	$t_{st}$
P1	30	3.0	3.0
P2	35	3.0	3.0
P3	40	3.0	3.0
P4	35	2.5	2.5
P5	35	3.5	3.5

Fig. 3. Schematic and geometric parameters of the orthogrid stiffened panels, with  $a = 100$  mm,  $b = 65$  mm and 5 combinations of  $h$ ,  $t_{sk}$  and  $t_{st}$ .



(a) Four point bending test rig (unit: mm).



(b) Upper rollers of the test rig (unit: mm).

Fig. 4. Four point bending test rig for buckling tests of stiffened panels.

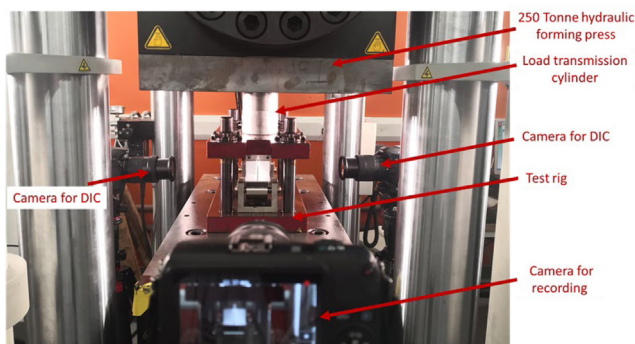


Fig. 5. Experimental setup for buckling tests with DIC system.

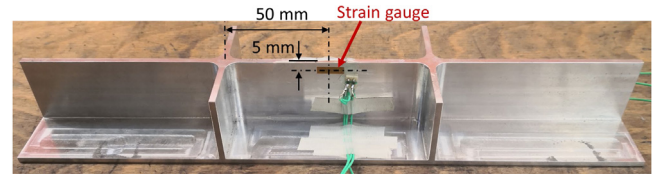


Fig. 6. Strain gauge measurement system setup and strain gauge location.

**3. Finite element simulations**

FE simulations for buckling analysis of the same setup was carried out at room temperature and ageing temperature considering the change of material properties with the temperature, using a commercial software Abaqus/Standard. The results are compared with the experimental investigations to determine the effectiveness of the FE modelling. The creep-ageing behaviour of the material was ignored in the FE simulations, since the whole stress field of stiffened panel decreased at the creep-ageing stage due to the stress relaxation, thus buckling was restrained, which was confirmed by the experimental results presented later.

The corresponding FE model and its boundary condition were shown in Fig. 7, closely representing the experimental environment. The upper and bottom rollers were simplified with the half of the roller surfaces with radii of 10 and 25 mm, respectively, which were modelled by discrete rigid shell elements (R3D4). The stiffened panel specimen located between the upper and bottom rollers was modelled by 4-node shell elements with reduced integration (S4R) with 5 integration points across the thickness of stiffener and skin since S4R elements can solve large-scale buckling problems efficiently in Abaqus/Standard and obtain accurate solutions [38]. The bottom rollers were fixed in all three directions as supporters, and the upper rollers were fixed in the  $x$ - and  $z$ -directions and could be pressed only in the  $y$ -direction to bend the specimen. For the boundary condition of the specimen, two ends of the longitudinal stiffener were fixed in the  $z$ -direction, and the middle line of the skin was fixed in the  $x$ -direction, as shown in Fig. 7, where  $U_x$ ,  $U_y$  and  $U_z$  are the translation in the  $x$ -,  $y$ - and  $z$ -directions. The surface-to-surface contact pair were built between (i) the upper rollers and top surface of the specimen; (ii) the bottom rollers and bottom surface of the specimen. The penalty friction formulation was used for the contact pair, and the friction coefficient between the rollers and the specimen is set as 0.1. The convergence study of mesh size was conducted for this model to capture accurate prediction of buckling stress efficiently, the mesh size of the specimen and rollers are both set as 2 mm, and the mesh of a part of FE model is also shown in Fig. 7. The material properties of AA7050-T7451 were applied for the FE model, in which Young's modulus and Poisson's ratio were 68 GPa and 0.33, respectively, for both room temperature and ageing temperature. The plasticity properties of the material at the two temperatures shown in Fig. 2 were inputted in the FE model.

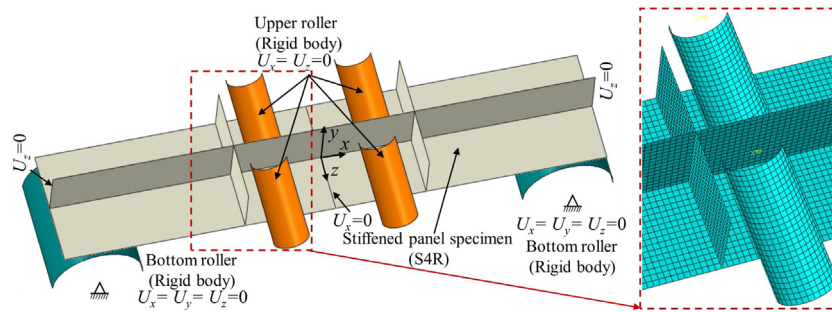
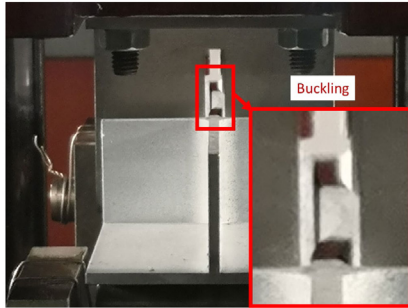
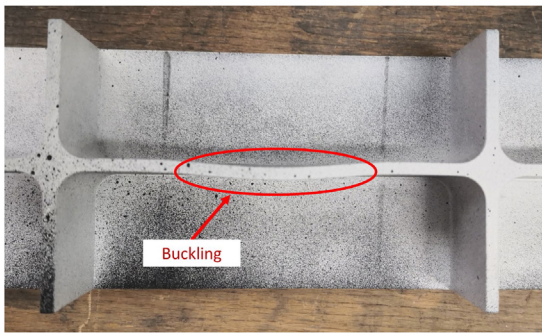


Fig. 7. FE model and mesh of stiffened panel under four point bending.



(a) Buckling mode shape under loading (specimen P1)



(b) Buckled stiffener shape after four point bending test (specimen P1)

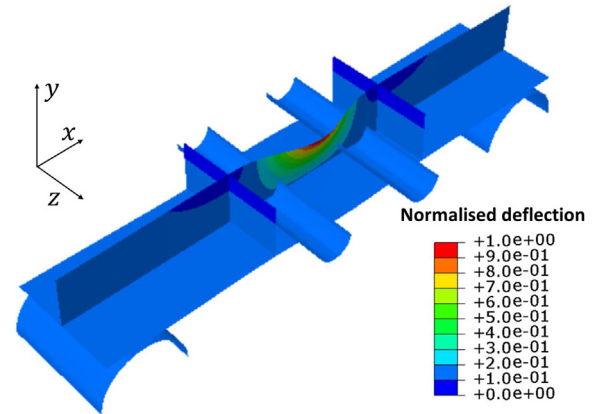
Fig. 8. Experimental buckling mode of stiffened panel under four point bending.

The FE simulation of buckling test for stiffened panel under four point bending was divided into three stages:

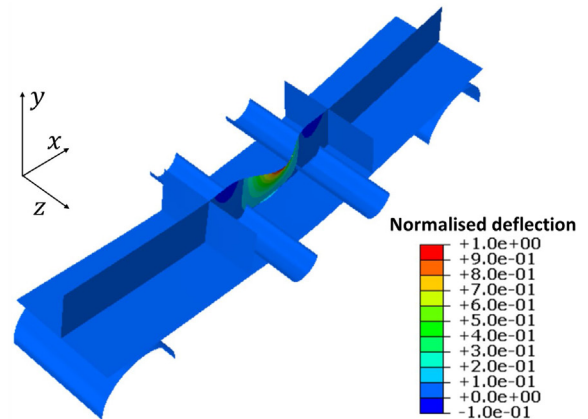
- (1) Gravity stage: the gravity was applied on the stiffened panel specimen to generate the initial contacts between the specimen and the bottom rollers.
- (2) Pre-loading stage: the upper rollers were displaced by  $-0.1\text{mm}$  in the  $y$ -direction to generate the initial contacts between the specimen and the upper rollers.
- (3) Buckling stage: a load along the  $y$ -direction was applied on the upper rollers to bend the specimen.

In this study, eigenvalue FE simulations were first carried out to capture the first-order buckling mode of stiffened panels under bending.

Non-linear FE simulations with the initial geometric imperfection, which was the deflection of the obtained first-order buckling mode from the eigenvalue FE simulations with a magnitude of 0.2% stiffener thickness in this study, were then conducted to obtain the buckling behaviour of stiffened panels subjected to four point bending, including buckling mode and buckling strain. The Riks method (arc-length



(a) Eigenvalue FE buckling analysis (specimen P1)



(b) Non-linear FE buckling analysis (specimen P1)

Fig. 9. Buckling mode of stiffened panels from both eigenvalue and non-linear FE methods.

method) was used in the non-linear buckling analysis to avoid non-convergence of the simulation due to the snap-through behaviour near the bifurcation point, in which the incremental values of loading and displacement can be adjusted simultaneously in one iteration [19].

#### 4. Results and analysis

In this section, experimental results, together with FE simulation results, for the buckling mode, the buckling stress and the buckling strain of stiffened panels under bending at room temperature and in CAF are reported and discussed.

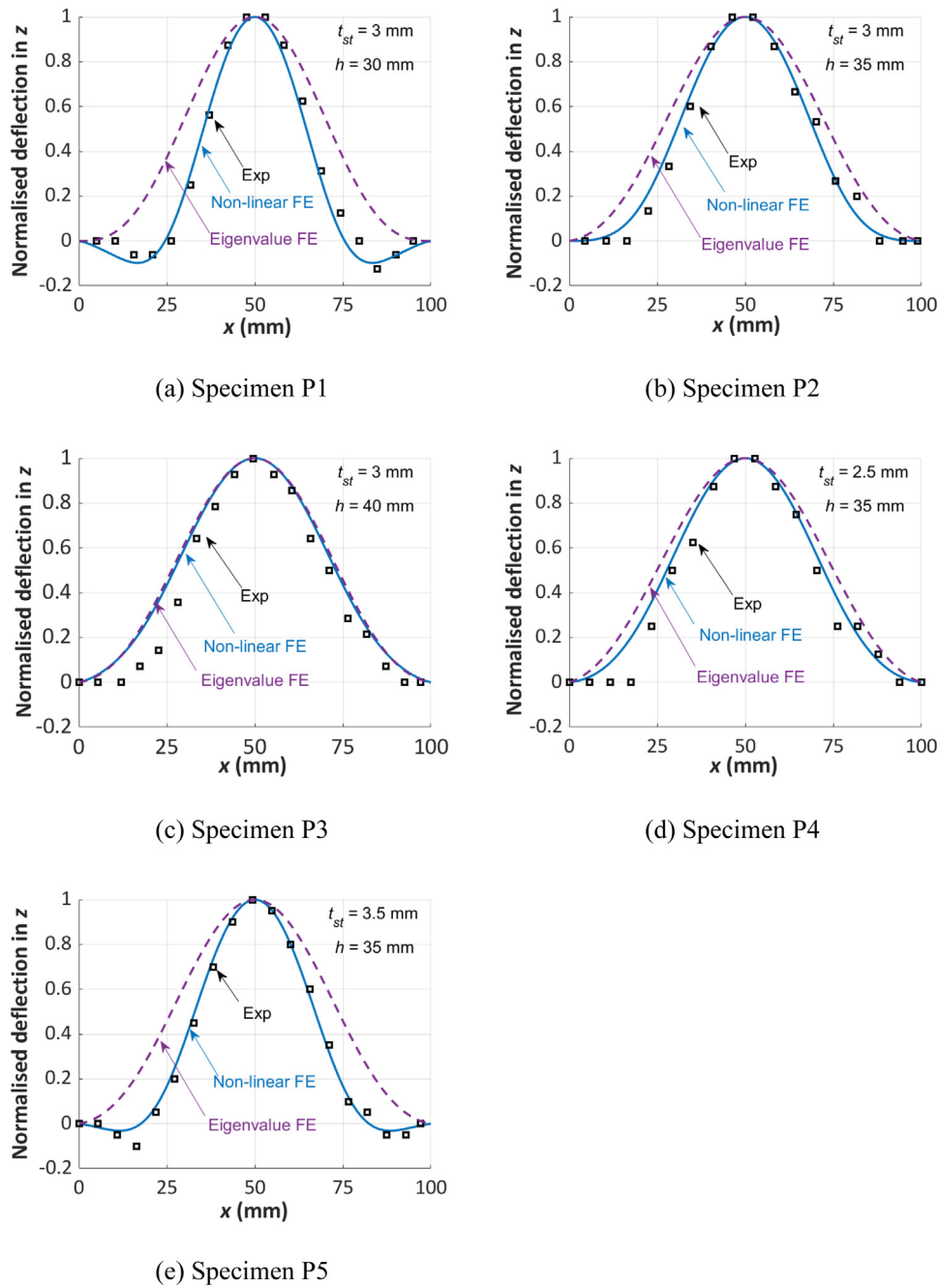


Fig. 10. Comparison of buckling mode of stiffened panels between experiments (symbols) and both eigenvalue and non-linear FE methods (curves) for specimens P1–P5 respectively.

4.1. Buckling behaviour at room temperature

This subsection reports the buckling test results at room temperature for five groups of stiffened panels with different geometry parameters. Corresponding FE simulations with the same geometry of the stiffened panel specimens used in the experiments were performed and compared with experimental results.

4.1.1. Buckling mode

Figs. 8(a) and 8(b) show the buckling mode shape of the stiffened panel under loading and after unloading in the experiments. They both show similar buckling mode shapes. The buckling mode of the stiffened panels under bending was stiffener buckling mode, in which buckling took place on the longitudinal stiffener between the two transverse stiffeners due to the concentration of high compression on the top of the

longitudinal stiffener, while there was no out-of-plane deformation on both sides of the longitudinal stiffener outside the transverse stiffeners. The longitudinal stiffener buckled in an approximate cosine mode according to Fig. 8. During the loading process, due to the obstruction of the test rig, the image of buckling mode shape of stiffened panels can only be obtained from the side of the stiffened panels and the buckling mode shape cannot be viewed from above. Therefore, the buckling mode shape after unloading was used to investigate the buckling mode of the stiffened panel under bending in this study and the results will be discussed later. It should be noted that this requires the plastic deformation of the stiffener for buckling to be visualised.

The buckling mode was also investigated using eigenvalue FE buckling analysis and non-linear FE buckling analysis. Fig. 9 shows the buckling modes of the stiffened panel under bending obtained from the two FE methods with the distribution of normalised deflection.



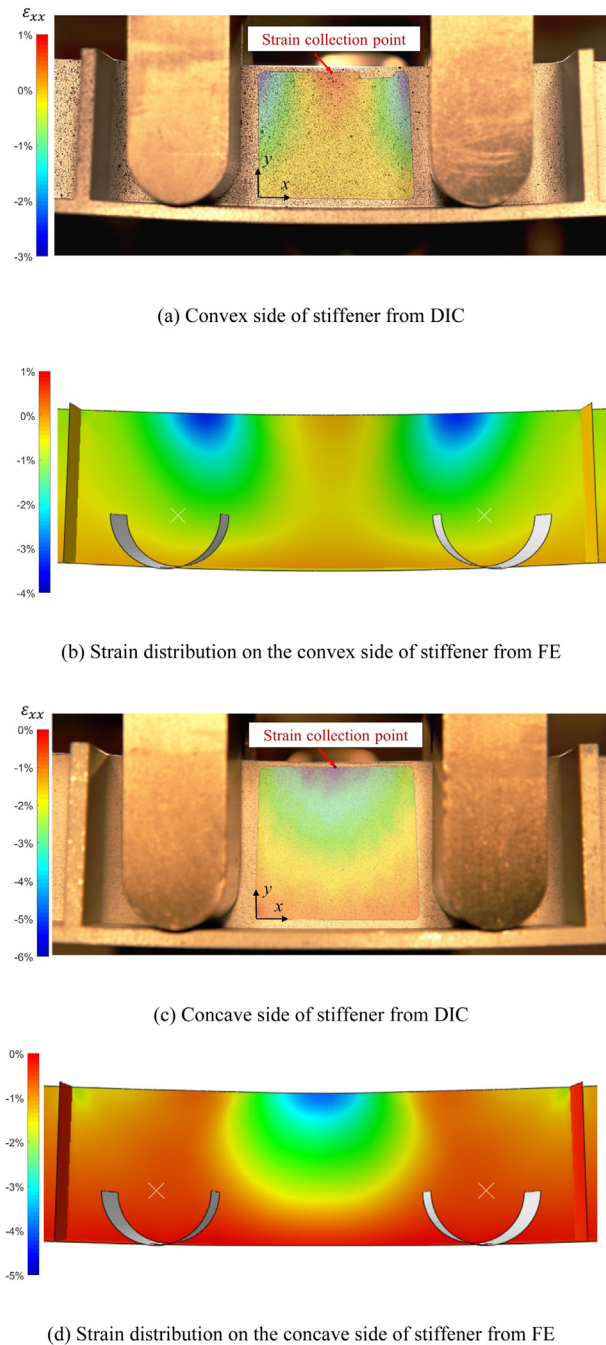


Fig. 11. Strain distribution on the longitudinal stiffener from DIC and FE simulations after buckling (specimen P1).

The normalised deflection was defined as the deflection in the  $z$ -direction (out-of-plane deformation) divided by the difference between the maximum deflection and the deflection of the two connections between longitudinal and transverse stiffeners. The minimum value of the normalised deflection was 0 at the two connections and the maximum value was 1. The stiffened panel under bending from both FE methods buckled in stiffener buckling mode which was similar with that from experimental results. As shown in Fig. 9, buckling mode shape from eigenvalue FE simulation only presents out-of-plane deformation without the deformation from four point bending, while the buckling mode shape from non-linear FE simulation includes the bending deformation and buckling deflection.

Fig. 10(a–e) show the comparison of the normalised deflection at the top of longitudinal stiffener between the two transverse stiffeners from eigenvalue FE simulations, non-linear FE simulations and the experiments, for the specimens P1–P5 respectively. The specimens P2, P3 and P4 show similar buckling mode shape with approximately one half-wave cosine mode; while for the specimens P1 and P5, the buckling modes were three half-wave cosine mode with two small opposite waves at the two sides of the stiffener, which indicates that the two transverse stiffeners provide finite rotation constraint to the ends of the longitudinal stiffener. From Fig. 10 and Table 2 which summaries the buckling stress for each specimen and is presented in the next subsection, it can be deduced that when the buckling stress increases from the elastic to the plastic region, the buckling mode shapes shrink to the middle area of longitudinal stiffener and change from one half-wave cosine mode to three half-wave cosine mode.

A good agreement of buckling mode between the non-linear FE results and the experimental results has been achieved, while the buckling modes from eigenvalue FE simulations were all one half-wave cosine mode. The eigenvalue FE results were close to the experimental results only for specimens P2–P4, which were in elastic buckling region. Since eigenvalue FE simulation ignores the deformation from four point bending and the plasticity of the material, the predictions of buckling mode shapes from non-linear FE simulations are more accurate than eigenvalue FE simulations, especially in the plastic region. The agreement between the non-linear results and experimental results indicates that using first-order buckling mode of eigenvalue FE buckling as the initial geometry imperfection of non-linear FE simulations was appropriate.

#### 4.1.2. Buckling stress and buckling strain

The strain distributions in the  $x$ -direction ( $\epsilon_{xx}$ ) of the two sides of the longitudinal stiffener obtained from DIC upon buckling are shown in Figs. 11(a) and 11(c), and the results from FE simulations are shown in Figs. 11(b) and 11(d) for comparison. As shown in Fig. 11, strain distributions of the two sides of the stiffener achieved a good agreement between experimental results and FE results. For strain at the convex side of the longitudinal stiffener upon buckling, the strain was relatively small on the middle of the stiffener and a tensile strain was observed at the upper middle area due to buckling, while large compressive strain was concentrated on the two sides of the upper area due to the two small negative half-waves from three half-wave cosine buckling mode. For the concave side of the longitudinal stiffener, compressive strain increased from the bottom to the upper of the stiffener and a large compressive strain was concentrated at the upper middle area while the compressive strain decreased from the middle to two sides of the upper area. The buckling strains were extracted at the middle point in the buckling zone at the upper edge (labelled strain collection point in Fig. 11), and the displacement of the upper rollers in the buckling tests was recorded from DIC.

Fig. 12 shows the experimental and FE results of the strains from two sides of the longitudinal stiffener versus displacement of upper rollers for specimens P1–P5. As shown in Fig. 12, for each group, strains from two sides of the stiffener decreased linearly with the increase of displacement of upper rollers and they were coincident before buckling occurs. The divergence of the strains from two sides of stiffener then took place, in which the strain from the convex side turned to increase while the strain from the other side continued to decrease with a larger slope, which indicates the buckling occurred. The buckling strain of stiffened panel specimens under four point bending is determined by the bifurcation point of the strains from two sides of the longitudinal stiffener, and was obtained from the strain evolution results by capturing the maximum magnitude of strain at the convex side of stiffener. The buckling strain and buckling stress values are summarised in Table 2. The buckling stress was obtained by the calculation with the buckling strain and the stress–strain curve. The stiffened panel specimens P2 ( $h = 35$  mm,  $t_{st} = 3.0$  mm), P3 ( $h = 40$  mm,



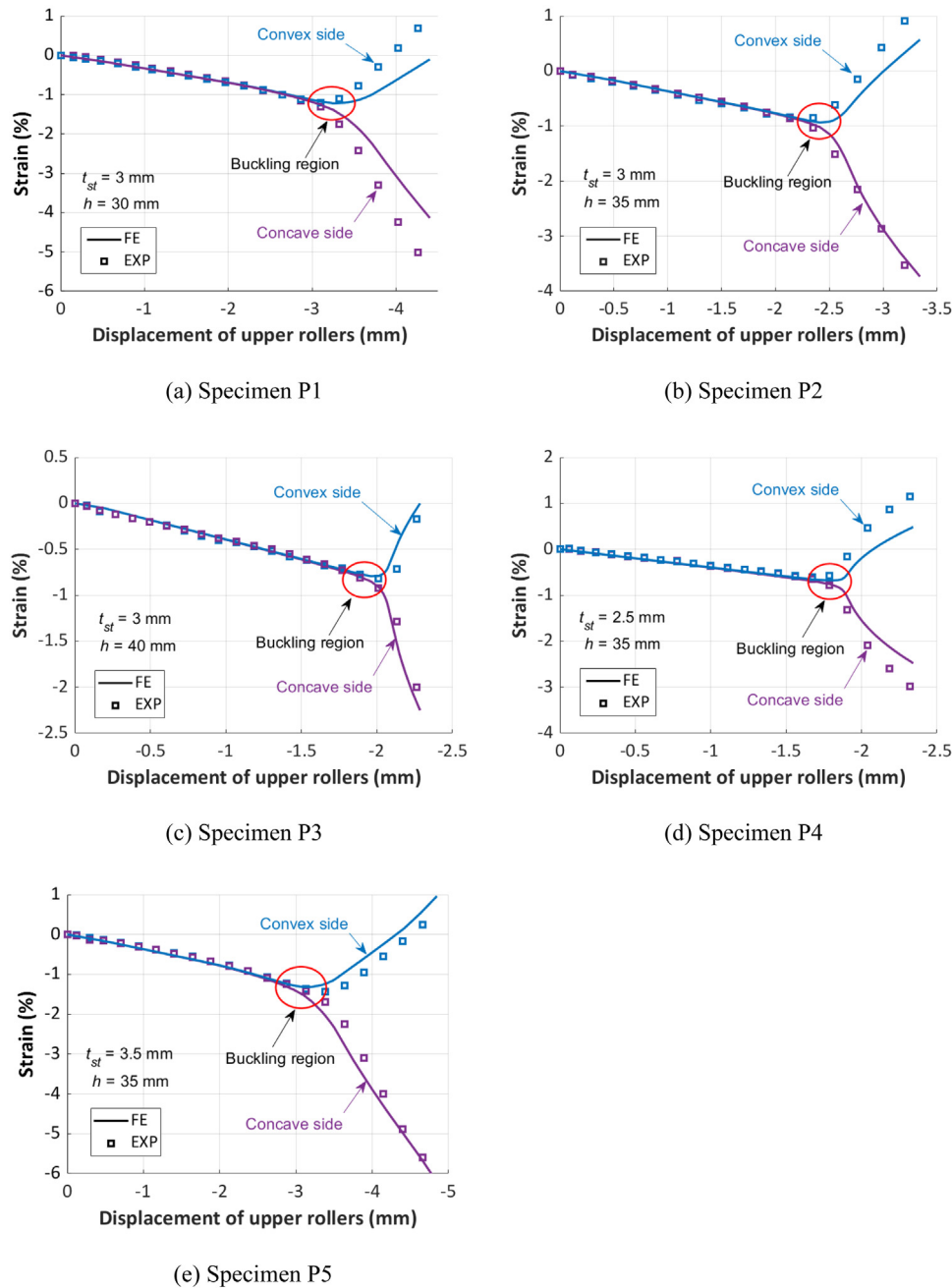


Fig. 12. Strain evolution on two sides of the longitudinal stiffener from DIC (symbols) and non-linear FE simulations (lines).

$t_{st} = 3.0$  mm) and P4 ( $h = 35$  mm,  $t_{st} = 2.5$  mm) buckled in the elastic region since the buckling stresses were below the yield stress of the material, the specimens P1 ( $h = 30$  mm,  $t_{st} = 3.0$  mm) and P5 ( $h = 35$  mm,  $t_{st} = 3.5$  mm) buckled in the plastic region. For buckling of stiffened panel under four point bending occurred in the elastic and plastic region, all experimental results of strain evolution show good agreements with the corresponding results from FE simulations. The difference of the buckling strain between the experimental and FE results was within 6.3% and the difference of the buckling stress was within 4.6%. The increase of stiffener thickness and decrease of stiffener height can improve the buckling resistance of stiffened panel, which is in agreement with the stiffened panel under uniform compression [28,39]. The buckling strain was increased by 119% when the stiffener thickness increased from 2.5 mm to 3.5 mm, and the buckling strain was increased by 54% when the stiffener height decreased from 40 mm to 30 mm.

## 4.2. Buckling behaviour in creep age forming process

### 4.2.1. Effect of heating and creep-ageing stages

Buckling tests of stiffened panels at room temperature with DIC and strain gauges were first conducted to compare the strain measurement performance of the DIC system and strain gauge. The results of strain from two sides of the longitudinal stiffener with two measurement methods are shown in Fig. 13. Since strain gauges were using for the buckling tests in the CAF process and the displacement of the upper rollers cannot be captured, the displacement from the forming machine was used to present the evolution of the strain of stiffened panels. Both strain results from DIC and strain gauge are in good agreement which indicates the strain gauges have the same measurements with DIC system.

**Table 2**  
Comparisons of buckling strain of stiffened panel test cases.

Panel no.	EXP buckling strain (%)	FE buckling strain (%)	Percentage difference <sup>a</sup> in strain	EXP buckling stress (MPa)	FE buckling stress (MPa)	Percentage difference in stress	Buckling
P1	-1.20	-1.22	1.8%	495	496	0.2%	Plastic
P2	-0.88	-0.93	5.7%	487	490	0.6%	Elastic
P3	-0.78	-0.79	1.7%	480	485	1.0%	Elastic
P4	-0.64	-0.68	6.3%	435	455	4.6%	Elastic
P5	-1.40	-1.32	-5.7%	498	497	-0.2%	Plastic

<sup>a</sup>Percentage difference = (FE result - EXP result)/EXP result × 100%.

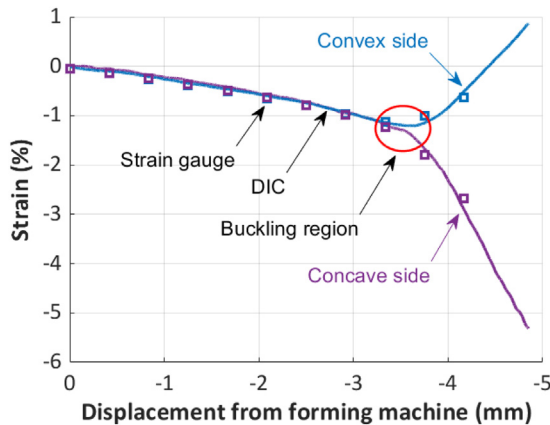


**Fig. 13.** Strain on two sides of the longitudinal stiffener from DIC (solid lines) and strain gauge (symbols).

The critical displacement of the loading plate of the forming machine for the buckling bifurcation point of the specimen P2 was obtained from buckling test at room temperature, which was 2.60 mm. As described in the experimental section, two sets of specimens were loaded to 90% and 100% of the critical displacement of the loading plate in the loading stage, as 2.34 mm and 2.60 mm, respectively, to investigate the effect of heating and creep-ageing stages in CAF on the buckling behaviour of stiffened panels. Then the specimens as well as the locked test rig were heated and creep-aged in the furnace. Fig. 14 presented the strains at the two sides of the longitudinal stiffener in the loading stage for the two sets of buckling tests. The compressive strains at the top of the stiffener increased linearly with the increase of the loading plate displacement during the loading stage for the two sets of tests. For the 90% loading tests, the strains at the two sides were coincident while a slight divergence of strains at the two sides can be observed at the end of the loading process for the 100% loading tests.

Fig. 15 shows the buckling responses of the stiffened panel specimens before and after heating and creep-ageing stages with 90% and 100% loading conditions. As shown in Figs. 15(a) and 15(c), the specimens with the two loading conditions had no obvious buckling before heating. After heating in the furnace, the specimen with 90% loading condition still did not have out-of-plane displacement, while buckling was observed on the longitudinal stiffener between two transverse stiffeners for the specimen with 100% loading condition in Fig. 15(d).

The strains with different loading displacements during the heating and creep-ageing stages in CAF are shown in Fig. 16(a). The strains at both sides of stiffener with 90% loading condition were close to each other. In the heating process, the compressive strains at both sides decreased as the temperature increased from the room temperature (20 °C) to about 80 °C, and then the compressive strains turned to increase until the temperature reached about 140 °C. Afterwards, the strain readings decreased gradually and continuously. At the end of the whole heating and creep-ageing process, the compressive strain readings slightly decreased compared with the starting condition. The strains at both sides with 100% loading condition present a different trend. The strain evolution of the convex side with 100% loading

condition was similar to that with 90% loading condition albeit at a higher magnitude, while the compressive strain of the concave side with 100% loading condition first slightly decreased then turned to increase sharply until the temperature reached about 140 °C, and finally, the strain remained fairly stable during the remaining heating and creep-ageing process, with a 0.018% strain decrease. To compensate for the effect of the temperature on the reading of the strain gauges, the difference of the strain at two sides of stiffener is calculated, as shown in Fig. 16(b), in which the temperature effects on the two strain gauges balance each other. The difference of the strains at two sides with 90% loading condition hardly changes during the heating and creep-ageing stages, which indicates that buckling did not occur on the longitudinal stiffener of the specimens in the whole process for the 90% loading condition. For the 100% loading condition, the difference of the strains increased sharply at the beginning of the heating process, and the difference continued to increase with a smaller rate and reached a relatively stable level during the creep-ageing stage, as 0.17% of strain, demonstrating that the buckling of the stiffened panel began and grew mainly during the heating process. This is presumably due to the changing material properties of the specimens at different temperatures.

#### 4.2.2. FE prediction for buckling behaviour at ageing temperature

The strains on the two sides at the top of the longitudinal stiffener and the average stress versus the displacement of upper rollers at room temperature and ageing temperature from FE simulations are shown in Fig. 17. The buckling of the stiffened panel at the two temperatures take place in the elastic-plastic region with the similar displacement of upper rollers. The strain evolutions at two sides of longitudinal stiffener show a similar trend for both room temperature and ageing temperature, while the stress evolution for the tests at the room temperature is higher than that for the tests at the ageing temperature in the plastic region due to the material property changing with temperatures. The buckling stress of the stiffened panel at the room temperature is higher than that at the ageing temperature, although the buckling strains of the stiffened panel at the two temperatures are close to each other, as 0.93% and 0.98% respectively for room temperature and ageing temperature. The buckling strain prediction from FE simulations reveals that buckling will not take place on this stiffened panel during the heating stage if buckling does not occur in the loading process, which is verified with the experimental results.

From the results and analysis above, increasing stiffener thickness or decreasing stiffener height increase the buckling stress of stiffened panels under four point bending. For the stiffened panel with the selected geometry, heating promotes the buckling of the stiffened panel only if the stiffened panel reaches the bifurcation point at the loading stage in the CAF. As demonstrated in the comparison with experimental results, the non-linear FE method achieves a high accuracy to the prediction of the buckling mode, the buckling strain and buckling stress of the stiffened panel under bending at the room temperature. The effect of the heating process in CAF on the buckling behaviour of stiffened panel can be predicted by the non-linear FE method considering the material property at the ageing temperature. In addition to the given cases, the non-linear FE method can be used to predict the formability limit by buckling of stiffened panels in a broad geometric range, which can be used to guide the design of stiffened panel to avoid possible buckling in both cold forming and CAF processes.

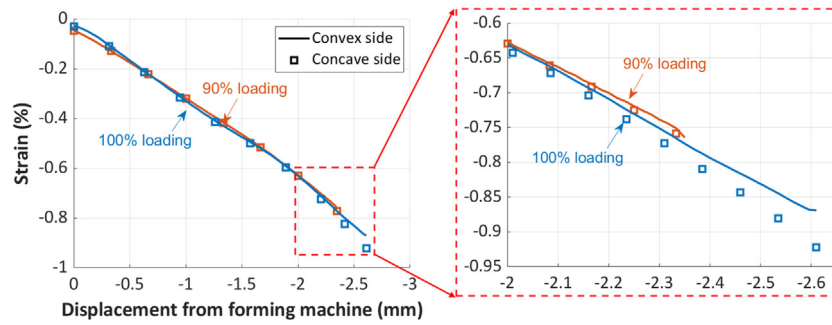


Fig. 14. Strain evolution on two sides of the longitudinal stiffener from strain gauges during the loading stage (specimen P2), with loading displacements of 90% and 100%.

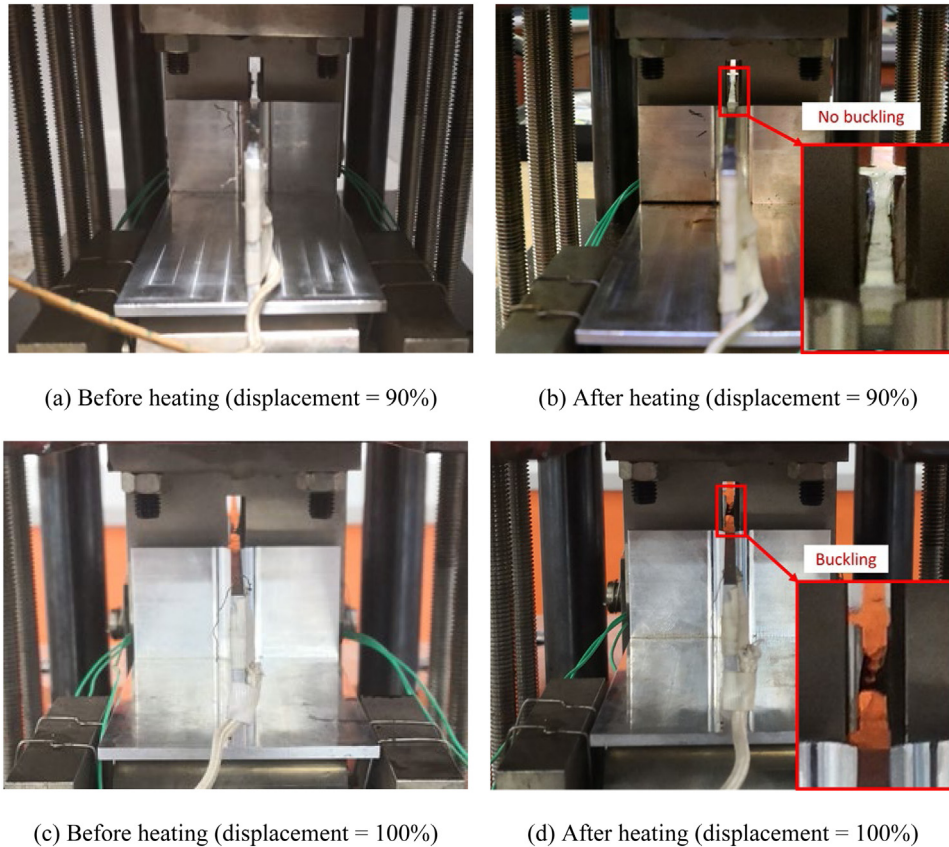
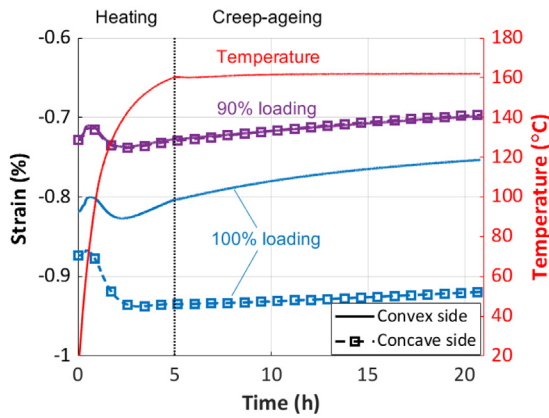


Fig. 15. Buckling responses before and after heating and creep-ageing stages for 90% and 100% of the critical displacement (specimen P2).

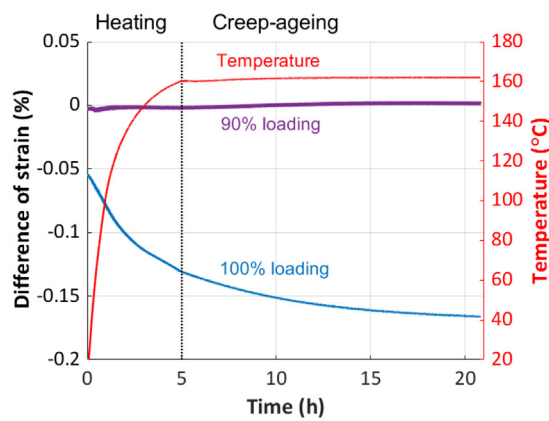
## 5. Conclusions

In this study, the buckling behaviour of stiffened panels subjected to four point bending during creep age forming has been experimentally and numerically investigated. Two sets of experiments have been carried out including the buckling tests of stiffened panels with different geometry parameters at room temperature and the buckling tests in the CAF with different loading degrees. The corresponding non-linear FE simulations have been conducted to compare with the results from the experiments and verify its effectiveness. The buckling mode, buckling strain and buckling stress for the stiffened panels under four point bending have been studied and the effect of the heating and creep-ageing stages on the buckling behaviour has been investigated. The following conclusions can be drawn:

- The buckling modes in the elastic region at room temperature are similar for all specimens and are one half-wave cosine mode, while the buckling modes transform to three half-wave cosine mode with two small deflections opposite to the main one in the plastic region. The buckling modes indicate that the two transverse stiffeners provide finite rotation constraints to the longitudinal stiffener.
- The formability limits by buckling are improved by the increase of stiffener thickness and/or the decrease of stiffener height. Increasing stiffener thickness from 2.5 mm to 3.5 mm or decreasing stiffener height from 40 mm to 30 mm increases the buckling strain by 119% and 54% respectively.
- The prediction of the buckling mode, the buckling strain and buckling stress of the stiffened panel at the room temperature from the non-linear FE method are in good agreement with experimental results with a maximum difference of 6.3%.
- During CAF, buckling does not occur on the stiffened panels with 90% loading condition but occurs on the specimen with 100% loading condition. The corresponding non-linear FE model using the material property at the ageing temperature can predict such



(a) Strain from two sides



(b) Difference of strain from two sides

Fig. 16. Strain evolutions on two sides of the longitudinal stiffener from strain gauges with 90% and 100% loading displacements during the heating and creep-ageing stages (specimen P2).

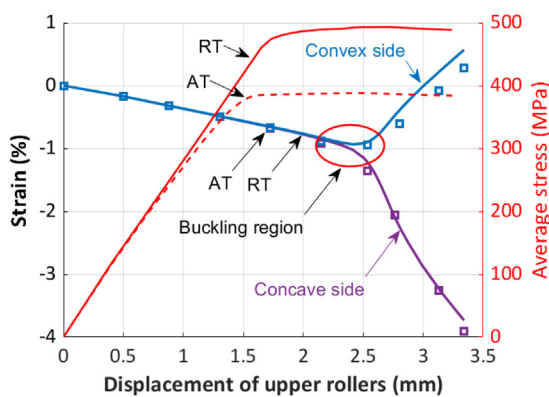


Fig. 17. Strain and average stress versus displacement of upper rollers from non-linear FE simulations at room temperature (solid lines) and ageing temperature (symbols).

buckling results during CAF. The buckling of the stiffened panel begins and grows mainly in the heating stage.

- When the temperature increases from room temperature to the ageing temperature, the buckling stress of stiffened panel decreases by 22%, while the buckling strain remains similar.

## CRediT authorship contribution statement

**Wenbin Zhou:** Methodology, Investigation, Writing – original draft. **Zhusheng Shi:** Conceptualization, Supervision, Funding acquisition, Writing – review & editing. **Qi Rong:** Investigation, Writing – review & editing. **Xuepiao Bai:** Writing – review & editing. **Yuansong Zeng:** Resources, Writing – review & editing. **Jianguo Lin:** Conceptualization, Supervision, Writing – review & editing.

## Declaration of competing interest

The authors declare that they have no known competing financial interests or personal relationships that could have appeared to influence the work reported in this paper.

## Acknowledgements

Financial support from the Aviation Industry Corporation of China (AVIC) Manufacturing Technology Institute (MTI) is gratefully acknowledged.

## References

- [1] J. Munroe, K. Wilkins, M. Gruber, M.S. Domack, *Integral Airframe Structures (IAS): Validated Feasibility Study of Integally Stiffened Metallic Fuselage Panels for Reducing Manufacturing Costs*, Report number, NASA/CR-2000-209337, Boeing Commercial Airplane Group, Seattle, Washington, 2000.
- [2] A.C.L. Lam, Z. Shi, H. Yang, L. Wan, C.M. Davies, J. Lin, S. Zhou, Creep-age forming AA2219 plates with different stiffener designs and pre-form age conditions: Experimental and finite element studies, *J. Mater. Process. Technol.* 219 (2015) 155–163, <http://dx.doi.org/10.1016/j.jmatprotec.2014.12.012>.
- [3] Y. Yang, L. Zhan, Forming characteristics of AA2219 integrally-stiffened plate subjected to creep age forming, *Procedia Manuf.* 15 (2018) 1000–1007, <http://dx.doi.org/10.1016/J.PROMFG.2018.07.394>.
- [4] Y. Yang, L. Zhan, R. Shen, J. Liu, X. Li, M. Huang, D. He, Z. Chang, Y. Ma, L. Wan, Investigation on the creep-age forming of an integrally-stiffened AA2219 alloy plate: experiment and modeling, *Int. J. Adv. Manuf. Technol.* 95 (2018) 2015–2025, <http://dx.doi.org/10.1007/s00170-017-1248-3>.
- [5] F. Lyu, Y. Li, X. Huang, Z. Shi, Y. Zeng, J. Lin, An investigation of creep age forming of AA7B04 stiffened plates: Experiment and FE modelling, *J. Manuf. Process.* 37 (2019) 232–241, <http://dx.doi.org/10.1016/J.JMAPRO.2018.11.031>.
- [6] D. Guines, A. Gavrus, E. Ragneau, Numerical modeling of integrally stiffened structures forming from creep age forming technique, *Int. J. Mater. Form.* 1 (2008) 1071–1074, <http://dx.doi.org/10.1007/s12289-008-0204-z>.
- [7] A.C.L. Lam, *A Flexible Tool Design and Integrated Modelling Techniques for Springback Compensation in Creep-Age Forming* (Ph.D. thesis), Imperial College London, 2015.
- [8] Y. Yan, M. Wan, H. Wang, Prediction of stiffener buckling in press bend forming of integral panels, *Trans. Nonferrous Met. Soc. China.* 21 (2011) 2459–2465, [http://dx.doi.org/10.1016/S1003-6326\(11\)61037-6](http://dx.doi.org/10.1016/S1003-6326(11)61037-6).
- [9] S. Zhang, I. Khan, Buckling and ultimate capability of plates and stiffened panels in axial compression, *Mar. Struct.* 22 (2009) 791–808, <http://dx.doi.org/10.1016/J.MARSTRUC.2009.09.001>.
- [10] T. Nguyen-Thoi, T. Bui-Xuan, P. Phung-Van, H. Nguyen-Xuan, P. Ngo-Thanh, Static, free vibration and buckling analyses of stiffened plates by CS-FEM-DSG3 using triangular elements, *Comput. Struct.* 125 (2013) 100–113, <http://dx.doi.org/10.1016/J.COMPSTRUC.2013.04.027>.
- [11] M. Mukhopadhyay, A. Mukherjee, Finite element buckling analysis of stiffened plates, *Comput. Struct.* 34 (1990) 795–803, [http://dx.doi.org/10.1016/0045-7949\(90\)90350-B](http://dx.doi.org/10.1016/0045-7949(90)90350-B).
- [12] O.F. Hughes, B. Ghosh, Y. Chen, Improved prediction of simultaneous local and overall buckling of stiffened panels, *Thin-Walled Struct.* 42 (2004) 827–856, <http://dx.doi.org/10.1016/J.TWS.2004.01.003>.
- [13] M. Fujikubo, T. Yao, Elastic local buckling strength of stiffened plate considering plate/stiffener interaction and welding residual stress, *Mar. Struct.* 12 (1999) 543–564.
- [14] N. Liu, H. Yang, H. Li, S. Yan, Plastic wrinkling prediction in thin-walled part forming process: A review, *Chinese J. Aeronaut.* 29 (2016) 1–14, <http://dx.doi.org/10.1016/J.CJA.2015.09.004>.
- [15] C. Lynch, A. Murphy, M. Price, A. Gibson, The computational post buckling analysis of fuselage stiffened panels loaded in compression, *Thin-Walled Struct.* 42 (2004) 1445–1464, <http://dx.doi.org/10.1016/j.tws.2004.04.002>.
- [16] M.C. Xu, D. Yanagihara, M. Fujikubo, C. Guedes Soares, Influence of boundary conditions on the collapse behaviour of stiffened panels under combined loads, *Mar. Struct.* 34 (2013) 205–225, <http://dx.doi.org/10.1016/J.MARSTRUC.2013.09.002>.



- [17] M.R. Khedmati, A. Bayatfar, P. Rigo, Post-buckling behaviour and strength of multi-stiffened aluminium panels under combined axial compression and lateral pressure, *Mar. Struct.* 23 (2010) 39–66, <http://dx.doi.org/10.1016/j.marstruc.2009.10.003>.
- [18] D. Quinn, A. Murphy, W. McEwan, F. Lemaitre, Non-prismatic sub-stiffening for stiffened panel plates-stability behaviour and performance gains, *Thin-Walled Struct.* 48 (2010) 401–413, <http://dx.doi.org/10.1016/j.tws.2010.01.010>.
- [19] R.M.F. Paulo, P. Carlone, R.A.F. Valente, F. Teixeira-Dias, F. Rubino, Numerical simulation of the buckling behaviour of stiffened panels: Benchmarks for assessment of distinct modelling strategies, *Int. J. Mech. Sci.* 157–158 (2019) 439–445, <http://dx.doi.org/10.1016/j.ijmecsci.2019.04.042>.
- [20] M.R. Khedmati, M.R. Zareei, P. Rigo, Sensitivity analysis on the elastic buckling and ultimate strength of continuous stiffened aluminium plates under combined in-plane compression and lateral pressure, *Thin-Walled Struct.* 47 (2009) 1232–1245, <http://dx.doi.org/10.1016/J.TWS.2009.04.010>.
- [21] J.W. Yoon, G.H. Bray, R.A.F. Valente, T.E.R. Childs, Buckling analysis for an integrally stiffened panel structure with a friction stir weld, *Thin-Walled Struct.* 47 (2009) 1608–1622, <http://dx.doi.org/10.1016/j.tws.2009.05.003>.
- [22] I.A. Sheikh, A.E. Elwi, G.Y. Grondin, Stiffened steel plates under combined compression and bending, *J. Constr. Steel Res.* 59 (2003) 911–930, [http://dx.doi.org/10.1016/S0143-974X\(02\)00079-2](http://dx.doi.org/10.1016/S0143-974X(02)00079-2).
- [23] W. Zhou, Q. Rong, Z. Shi, Y. Zeng, Non-linear finite element investigation of formability limit by buckling in creep age forming of stiffened panels, *Procedia Manuf.* 50 (2020) 625–629, <http://dx.doi.org/10.1016/j.promfg.2020.08.112>.
- [24] L. Boni, D. Fanteria, A. Lanciotti, Post-buckling behaviour of flat stiffened composite panels: Experiments vs. analysis, *Compos. Struct.* 94 (2012) 3421–3433, <http://dx.doi.org/10.1016/j.compstruct.2012.06.005>.
- [25] S. Zhu, J. Yan, Z. Chen, M. Tong, Y. Wang, Effect of the stiffener stiffness on the buckling and post-buckling behavior of stiffened composite panels – experimental investigation, *Compos. Struct.* 120 (2015) 334–345, <http://dx.doi.org/10.1016/j.compstruct.2014.10.021>.
- [26] N.R. Kolanu, G. Raju, M. Ramji, Experimental and numerical studies on the buckling and post-buckling behavior of single blade-stiffened CFRP panels, *Compos. Struct.* 196 (2018) 135–154, <http://dx.doi.org/10.1016/j.compstruct.2018.05.015>.
- [27] A. Aalberg, M. Langseth, P.K. Larsen, Stiffened aluminium panels subjected to axial compression, *Thin-Walled Struct.* 39 (2001) 861–885, [http://dx.doi.org/10.1016/S0263-8231\(01\)00021-0](http://dx.doi.org/10.1016/S0263-8231(01)00021-0).
- [28] Y. Mo, D. Ge, J. Zhou, Experiment and analysis of hat-stringer-stiffened composite curved panels under axial compression, *Compos. Struct.* 123 (2015) 150–160, <http://dx.doi.org/10.1016/j.compstruct.2014.11.074>.
- [29] B. Falzon, K. Stevens, G. Davies, Postbuckling behaviour of a blade-stiffened composite panel loaded in uniaxial compression, *Compos. A Appl. Sci. Manuf.* 31 (2000) 459–468, [http://dx.doi.org/10.1016/S1359-835X\(99\)00085-8](http://dx.doi.org/10.1016/S1359-835X(99)00085-8).
- [30] O. Zhao, L. Gardner, B. Young, Buckling of ferritic stainless steel members under combined axial compression and bending, *J. Constr. Steel Res.* 117 (2016) 35–48, <http://dx.doi.org/10.1016/j.jcsr.2015.10.003>.
- [31] X. Kong, Y. Yang, J. Gan, T. Yuan, L. Ao, W. Wu, Experimental and numerical investigation on the detailed buckling process of similar stiffened panels subjected to in-plane compressive load, *Thin-Walled Struct.* 148 (2020) 106620, <http://dx.doi.org/10.1016/j.tws.2020.106620>.
- [32] Y.L. Wang, Q.L. Pan, L.L. Wei, B. Li, Y. Wang, Effect of retrogression and reaging treatment on the microstructure and fatigue crack growth behavior of 7050 aluminum alloy thick plate, *Mater. Des.* 55 (2014) 857–863, <http://dx.doi.org/10.1016/j.matdes.2013.09.063>.
- [33] *ASTM E8/E8M-21: Standard Test Methods for Tension Testing of Metallic Materials*, ASTM International, West Conshohocken, PA, 2021.
- [34] *ASTM E21-17: Standard Test Method for Elevated Temperature Tension Tests of Metallic Materials*, ASTM International, West Conshohocken, PA, 2017.
- [35] J.H. Kim, S.B. Lee, Behavior of plasticity-induced crack closure and roughness-induced crack closure in aluminum alloy, *Int. J. Fatigue* 23 (2001) 247–251, [http://dx.doi.org/10.1016/S0142-1123\(01\)00155-4](http://dx.doi.org/10.1016/S0142-1123(01)00155-4).
- [36] W. Zhou, Y. Li, Z. Shi, J. Lin, An analytical solution for elastic buckling analysis of stiffened panel subjected to pure bending, *Int. J. Mech. Sci.* 161–162 (2019) 105024, <http://dx.doi.org/10.1016/J.IJMECSCI.2019.105024>.
- [37] W. Zhou, Z. Shi, Y. Li, Q. Rong, Y. Zeng, J. Lin, Elastic-plastic buckling analysis of stiffened panel subjected to global bending in forming process, *Aerosp. Sci. Technol.* 115 (2021) 106781, <http://dx.doi.org/10.1016/j.ast.2021.106781>.
- [38] *Abaqus User's Manual (6.10)*, Providence, RI, USA, 2010.
- [39] A. Murphy, W. McCune, D. Quinn, M. Price, The characterisation of friction stir welding process effects on stiffened panel buckling performance, *Thin-Walled Struct.* 45 (2007) 339–351, <http://dx.doi.org/10.1016/J.TWS.2007.02.007>.